DETAILED MEASUREMENTS OF LOCAL PARAMETERS IN ANNULAR TWO-PHASE FLOW IN FUEL BUNDLE UNDER BWR OPERATING CONDITIONS

J.-M. Le Corre, U. C. Bergmann, A. Hallehn, H. Tejne, F. Waldemarsson
Westinghouse Electric Sweden AB
72163 Västerås, Sweden
lecorrjm@westinghouse.com

B. Morenius
Royal Institute of Technology
10691, Stockholm, Sweden
morenius@kth.se

R. Baghai
RBI Instrumentation
38240, Meylan, France
rbi.sarl@wanadoo.fr

ABSTRACT

The Westinghouse FRIGG facility, in Västerås/Sweden, is dedicated to the measurement of critical power, stability and pressure drop in fuel rod bundles under BWR operating conditions (steady-state and transient). The facility is particularly relevant to test modern BWR fuel designs which typically have complex features, such as part-length rods and mixing vanes that make the flow heterogeneous and challenging to accurately simulate (e.g. using sub-channel analysis codes or CFD tools).

In order to support the validation of advanced thermal-hydraulics codes for detailed BWR fuel assembly simulation, new local instrumentation techniques have been tested at the FRIGG facility for the measurement of two-phase dynamic pressure (Pitot tubes) and high time resolution phase detection (optical sensor). The optical sensors were custom-made by RBI Instrumentation for the FRIGG facility and optimized for annular two-phase flow (drop/steam) under BWR operating conditions.

This new instrumentation was successfully tested and allows the first-time measurement, under BWR operating conditions, of relevant two-phase flow parameters such as the local void fraction in the steam core, the local drop/steam velocity, the volumetric interfacial area, the drop collision frequency and the assessment of drop size distribution during BWR steady-state and transient operations.

1. INTRODUCTION

The Westinghouse FRIGG facility has been used for nearly 50 years to perform full-scale BWR fuel thermal-hydraulic experiments under realistic steady-state and transient core conditions. The test results have supported the development of various successive BWR fuel designs and established the experimental basis for the development of Critical Power Ratio (CPR) correlations [1]. Beside dryout tests, the facility is also used for fuel assembly pressure drop measurements (single phase and two-phase) and stability tests.

In the past, the facility has been equipped with advanced instrumentation techniques to measure detailed void fraction distribution, e.g. using gamma tomography [2]. However, the use of this type of instrumentation is often cumbersome and requires the use of a radiation source. As an alternative, and to obtain further insight in the thermal-hydraulic behavior of a BWR fuel assembly, new instrumentations were recently tested at the FRIGG facility. The new measurements can be used for the development and validation of advanced thermal-hydraulics codes for detailed fuel bundle simulations.

2. FRIGG FACILITY

2.1. Test Loop Capabilities

The FRIGG facility is a full-scale BWR thermal-hydraulic test facility located in Västerås, Sweden. The facility has been operated since the 1960s to qualify a long series of BWR fuel designs, starting from the early 8x8 fuel lattice until the latest 10x10 SVEA-96 fuel designs. The loop was modernized and upgraded in 1995.

The FRIGG test facility is designed to cover all requirements for BWR fuel heat transfer and pressure drop testing under BWR two-phase flow conditions, including boiling transition (dryout) and thermal-hydraulic stability. The dryout tests are typically performed under a wide range of steady-state BWR operating conditions (flow, pressure, inlet temperature, axial power distributions). A wide range of variation in radial power distributions can also be achieved with the use of indirectly heated fuel rod simulators. In complement to steady-state tests, realistic transient dryout experiments can be performed with rapid power and flow variations.

The capability to measure cross-sectional void and radial void distributions during steady-state operation was considered when the facility was built in the late 1960s, using gamma transmission measurements. In the 1990s, redesigned equipment was installed to allow for full 2D tomography and some test campaigns were successfully run where the void was measured in the Westinghouse SVEA-96 fuel bundle geometry with and without part-length rods.

2.2. Test Loop Design and Instrumentation

The FRIGG loop is designed to operate at maximum of 10 MPa and 15 MW, sufficient for full-size BWR fuel assembly testing. The Westinghouse SVEA quarter-assembly can also be tested. Data collection of all relevant parameters is typically performed at 25 Hz. The FRIGG test section consists of a pressure vessel, a flow channel and a fuel bundle consisting of electrically heated fuel rod simulators and spacer grids. Pressure sensors are connected to the flow channel at different elevation taps. A schematic of the FRIGG test loop can be found in Figure 1.

The flow channels are manufactured in normal fuel channel production and are hence realistic (apart from the pressure taps). The same applies to the spacer grids, which are entirely without reinforcements. Use of standard components is possible in FRIGG due to the use of the "indirect" heater rods that eliminates the

need for electrically insulating flow channel ceramics. More detailed information regarding the FRIGG loop design can be found in [1].
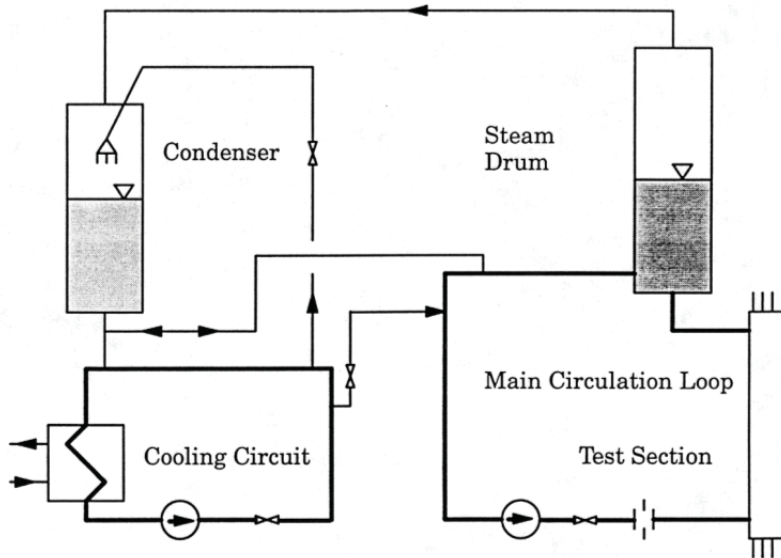

Figure 1. FRIGG test loop

Rapid control of power and flow is possible, to simulate typical limiting safety-related BWR transients, such as flow reduction during a pump trip, rapid power increase transients or a combination of both. The transient forcing functions are introduced from pre-calculations via a control computer.

The FRIGG data acquisition system consists of a main computer and a number of scanners, allowing the simultaneous collection of up to 830 signals at 25 Hz. The data recording and control systems have been continuously upgraded to meet current standards.

Void measurement using gamma tomography has been a very important testing objective, from the early HWR and BWR lattices, until the current 10x10 lattices. A new tomography system was developed and used for advanced 10x10 fuel validation [2], including to investigate the effects of part-length fuel rods [3]. The databases from void measurements have been used to validate the void correlations needed in the core design methods. The early HWR FRIGG data were published and are available in the open literature (e.g. in [4]).

3. NEW LOCAL INSTRUMENTATION

3.1. Objectives

Modern BWR fuel assemblies include features that can make the flow inhomogeneous and challenging to simulate with available TH simulation tools (validated mainly in single channels and homogeneous fuel lattices). At the end of the part-length rods, typical of modern BWR fuel designs, sudden expansions of the flow area are created, leaving place to empty regions within the fuel lattice. This can lead to significant cross flows which can be challenging to simulate accurately, in particular when considering separately the film, drop and steam fields, typical of annular two-phase flow.

The measurement of relevant local flow information is required to validate sub-channel and CFD codes. Under typical BWR conditions, the flow regime of interest is annular flow where a thin liquid film flows over the walls and the steam core is mixed with liquid droplets. The liquid film flow would be very challenging to measure in a high pressure / high temperature test rig. However, it is possible to position local probes for the measurement of relevant two-phase flow parameters in the steam core (i.e. away from the rods and channel box). For that purpose, The FRIGG facility has been equipped with Pitot tubes (Section 3.2), for two-phase dynamic pressure measurement, and optical sensors (Section 3.3), for local phase detection. When used together, these instruments allow for the measurements of local void fraction, flow velocity and drop diameter distribution in the two-phase steam core.

Both instruments are intrusive and perform local measurements. They were placed downstream, but close to, the end of heated length (EOHL) and hence had no effect on dryout and pressure drop measurements within the heated length. In the results presented in this work, both instruments were placed in the open region above part-length rods.

3.2. Pitot Tubes

3.2.1. Measurement principles

Pitot tubes are commonly used to measure local dynamic pressure and fluid velocity in liquid, air and gas flow for many industrial applications (e.g. aircraft or boat speed). Though most applications are performed under single-phase flow conditions, applications to two-phase flow are also possible under specific assumptions. Some applications under gas/liquid and liquid/liquid two-phase flows can be found in [5], [6] and [8].

A Pitot tube is composed of 2 ports, the first port faces the flow direction and measures the stagnation (total) pressure of the fluid (P_t, static + dynamic). The second port is typically perpendicular to the flow direction and measures the static pressure (P_s). In two-phase flow, the pressure difference between the two ports is hence

$$\Delta P = P_t - P_s \approx \left[(1 - \alpha) \frac{\rho_L V_L^2}{2} + \alpha \frac{\rho_G V_G^2}{2} \right] \tag{1}$$

where α is the void fraction, ρ_L the liquid density, ρ_G the gas density, V_L the liquid velocity and V_G the gas velocity. Under the assumptions that the velocity slip between liquid and gas is negligible (i.e. $V_L \approx V_G \approx V$), then

$$\Delta P \approx \frac{\rho_{mix} V^2}{2} \tag{2}$$

where the mixture density (ρ_{mix}) is calculated as follows

$$\rho_{mix} = (1 - \alpha)\rho_L + \alpha \rho_G \tag{3}$$

Assuming that the void fraction at the same location is known, the flow velocity can then be calculated

$$V \approx \sqrt{\frac{2\Delta P}{\rho_{mix}}} \tag{4}$$

However, available void correlations are not adequate to predict the local void in the steam core and a direct measurement is necessary. In [5] and [7], the Pitot measurements were coupled with void fraction

measured using a gamma densitometer (chordal average). This technique to measure a local void fraction is not practical for the FRIGG facility due to a thick pressure vessel and complex geometry. An alternative technique is presented in Section 3.3.

3.2.2. Installation

The Pitot tube starts from the pressure transmitter, up to the top of the pressure vessel (about 1 meter) and down through the top flange and (about 800 mm) to the EOHL (Figure 3), where the measurements of total and static pressure are performed. This particular setup could result in a situation where the tubes are not always filled with water, which would lead to a faulty pressure drop reading. To prevent this, a gear pump has been included in the installation that can be used to fill the pipes. In practice, it is not necessary to run the gear pump often. This is typically performed routinely once a day during the tests.

3.2.3. Data acquisition

The differential between total and static pressure is measured using a pressure transmitter with a measurement range of 0 to 60 kPa. The new instrument is integrated in the main FRIGG data acquisition system and the measurement is performed continuously at a rate of 25 Hz.

3.3. Optical Sensor

Different techniques can be used to measure the void fraction in a two-phase flow system. Non-intrusive techniques typically consist of tomographic methods using gamma rays, X rays or neutron attenuation. Intrusive techniques can consist of conductivity probes, optical probes, wire-mesh sensors, hot-wire anemometers, etc. Void measurements with gamma densitometers, used in complement to Pitot tube measurements, can be found in [5] and [7]. However, under typical BWR conditions, severe restrictions are imposed due to high pressure and temperature conditions.

Following a review of available instrumentation techniques, and accounting for the specific operating conditions of the FRIGG loop, a single-sensor optical probe technique was selected for the test. The high accuracy of this technique for interface detection and measurement of local void fraction has been demonstrated for more than 40 years (e.g. in [9]). Later, the use of multi-sensor techniques has allowed the measurement of additional two-phase flow parameters such as velocity and volumetric interfacial area (e.g. in [10] and [11]). The selected probe is manufactured by RBI Instrumentation and the single sensor tip is made of sapphire which is designed to sustain the high pressure and temperature, typical of BWR operation (P=70 bar, T_{sat} = 285 C). Detailed characteristics of the sapphire probe are documented in [12]. Use of multi-sensor technique was not considered for annular two-phase flow since the distance between the sensors cannot be practically small enough, with respect to the dimension of the expected drops. Measurement principles of a single-sensor probe, installation and data acquisition are summarized in the following sections.

3.3.1. Measurement principles

Optical sensor probes utilize the discrete variation of the refraction index between liquid and gas to identify which phase is in contact with the tip of the sensor. A laser light is emitted into the optical fiber by an opto-electronic module, the light will either reflect or diffract depending on its angle of incidence and the index of refraction of the fluid in contact with the sensor, which acts as a Descartes prism, Figure 2. The conversion of the returning optical signal into an electrical signal is ensured by a photo-sensitive element. The response time of the system to a phase change is very short (< 1μs) which makes it relevant to capture individual drops in annular two-phase flow (see discussion in Section 4.2.2).
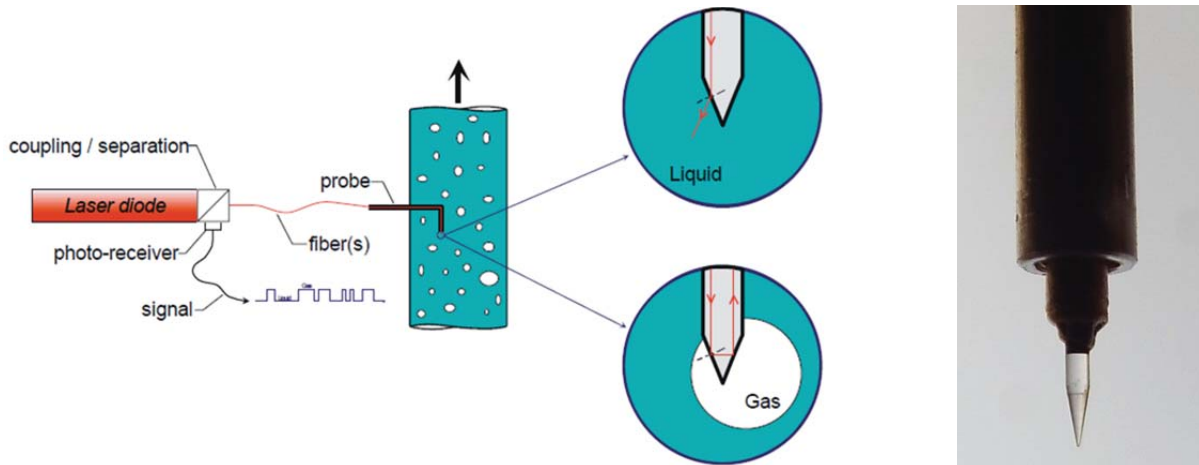
Figure 2. Optical probe functioning principles (bubbly flow, left) and sapphire optical probe used at FRIGG (right). Images courtesy of RBI.

The tip of the probe, made of sapphire, is about 30 μm wide hence one order of magnitude smaller than the expected drop size (see drop size measurements in Section 5). This is an important factor to ensure that the sensor does not significantly affect the local flow conditions.

3.3.2. Installation

The optical probe used for void measurements in the FRIGG loop is inserted from the top of the test section, through a tapped hole in the top flange, down into the fuel bundle. The tapped holes can be located above a part-length rod or in between full-length rods, according to the desired radial position. In order to seal off the probe and the test vessel, which holds around 70 bar during tests (and up to 140 bar during pressure tests), a gasket made out of graphite material is used. The graphite gasket sits at the bottom tapped hole so that when the probe is inserted it gets compressed hence creating the sealant.

Figure 3. Pitot tube and optical probes installation inside the test bundle (at EOHL)

Inside the test section, the probe is guided via a pre-installed vertical tube which protects the tip during the insertion. The length of the body of the probe is specifically designed so that its tip sits at EOHL when sealed into the top flange, Figure 3.

3.3.3. Data acquisition

The acquisition of optical sensor data is separate from the main FRIGG data acquisition system. The opto-electronic module sends and receives the laser signal from each probe. The module has a 20 MHz bandwidth and the zero and gain of the signal can be manually adjusted. Typically the signal is set at 0 V in the liquid phase and 5 V in the steam phase. The raw signal can be visually observed via a PC-based oscilloscope, Figure 4. The opto-electronic module also "shapes" the raw signal into a binary signal (TTL) using manually adjustable low and high threshold levels. This allows to accurately record the time of phase change and avoid capturing any noise from the raw signal. The binary signal is sent to a dedicated acquisition board which can allow up to 16 input channels and runs at 20 MHz scanning frequency, corresponding to a maximum time resolution of 0.05 μs. The acquisition board also sends an acquisition on/off signal to the main FRIGG acquisition system so that the time stamps of both the FRIGG acquisition data and optical probe acquisition data can be matched in post-processing.

Both the raw and binary signals, over a time period of a few milliseconds, can be observed in Figure 4. Passing drops can be clearly observed when the signal rapidly falls and rises over a period of a few microseconds. It can be observed that the binary signal accurately "shapes" the raw signal without loss in drop counts and liquid presence time.
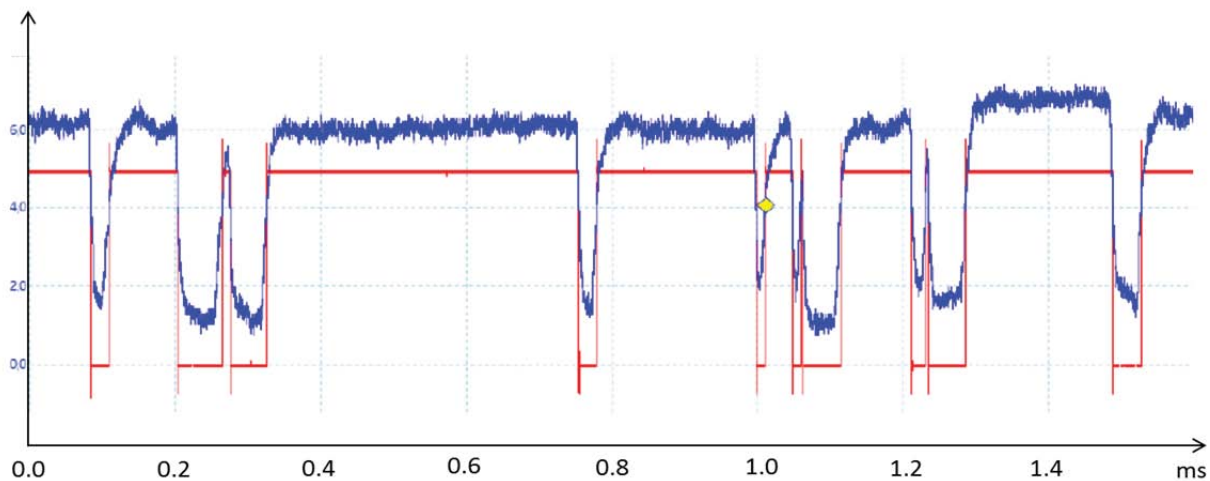

Figure 4. Time-dependent raw signal seen by the opto-electronics module and corresponding binary signal collected by the acquisition board

Based on the experience from several test campaigns using optical probes at the FRIGG facility, a degradation of the signal (lower gain) has been systematically observed after several days of operation. Post-test inspections have shown that the tip of the probe erodes, hence reducing the amount of light returning to the photo-sensitive element. In order to address this issue, development work is currently in progress to replace the sapphire material by diamond.

4. DATA-PROCESSING

4.1. Pitot Tubes

The dynamic pressure is directly measured as a pressure difference between the total and static pressure ports of the Pitot tube by a differential pressure sensor. This pressure difference is read by the main FRIGG acquisition system at a 25 Hz frequency. The use of the measured dynamic pressure to calculate the flow velocity is documented in Section 3.2.1.

4.2. Optical Sensor

4.2.1. Time-averaged void fraction and flow velocity

The post-processing of the optical probe signal can be performed with the RBI software ISO, or alternatively, with a dedicated post-processing script. The latter option is more relevant in the case of the FRIGG applications to automate the coupling with the data acquired by the main FRIGG system (in particular from Pitot tubes). Using a post-processing script, the signals from the main FRIGG acquisition system are averaged and paired with the optical probe signal recorded during the exact same time. The averaging is typically made in 20 seconds intervals under stable conditions (e.g. when a dryout point or a two-phase pressure drop point is recorded). Over the relevant time range, the binary phase indicator signal is time-averaged to calculate the measured local void fraction (α)

$$\alpha = \frac{1}{T}\sum_{k=1}^{N_b}(\Delta t_g)_k \qquad (5)$$

where T is the sampling time (typically, 20 sec), N_b is the number of events and Δt_g is the steam residence time for an event. Once the local void fraction is known, the mixture density and flow velocity can be calculated according to Equations (3) and (4), respectively. Results for selected tests are presented in Section 5.

4.2.2. Drop residence time and size distributions

Beyond local void fraction and flow velocity, which are based on the time-average of the phase indicator signal, additional relevant quantities can be estimated by considering the distribution of drop residence time and drop collision frequency with the sensor.

Drop residence time distribution is first considered, using a bin size of 2 µs, corresponding to the smallest liquid inclusion that can be reasonably measured by the instrument. When multiplying the drop inclusion time by the flow velocity (Equation 4), under the assumption that there is a negligible slip between steam and drops, the drop chord length distribution can be calculated, Figure 5.
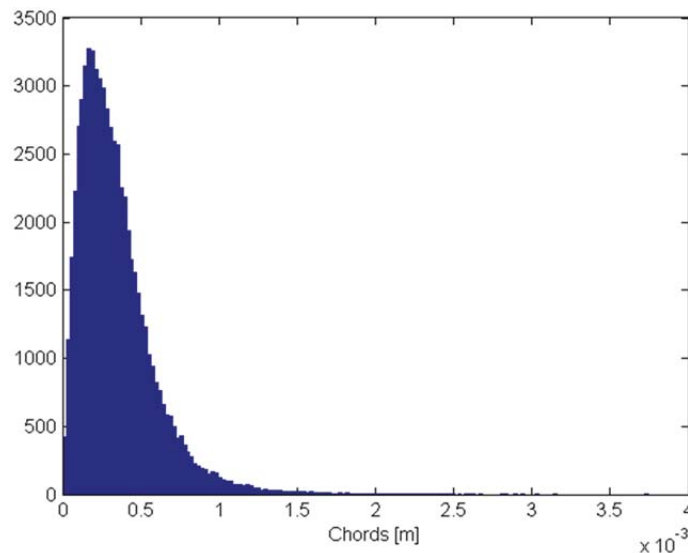

Figure 5. Example of drop chord length histogram

Assuming a spherical drop shape (which seems reasonable under the considered pressure and expected drop sizes), the drop diameter distribution (P_d) can be calculated from the drop chord length distribution (P_{dc}) by inverting the following equation [13]:

$$P_{d_c} = AP_d \qquad (6)$$

where A is a transition matrix from particle chord length to diameter [13]. A is composed of conditional probabilities, that is, probabilities of sampling a particular chord length given a certain drop diameter. Having the experimentally obtained chord lengths (P_{dc}) and the analytically generated transition matrix A, there may not be an exact solution (P_d) for the drop size distribution which satisfies Equation (6). However, P_d can be approximated by $\widehat{P_d}$ which best fits the equation, using the least squares method:

$$\widehat{P_d} = (A^T A)^{-1} A^T P_d \qquad (7)$$

In the case where $A^T A$ is not invertible or the chord length distribution is noisy, the system can be ill-conditioned and the constrained least squares method [13] is used instead:

$$\widehat{P_d} = (A^T A + \lambda I)^{-1} A^T P_d \qquad (8)$$

where I is the identity matrix and λ is a smoothing parameter. Typically, λ is chosen to be a small positive value (0.5). Note that the method does not make any assumption on the shape of the measured chord length distributions.

4.2.3. Characterization of the measured drop size distributions

When it comes to describing a particle size (d) distribution, it is typical to measure it in term of either a number, surface or volume basis. That is, the distribution can show the number of particles within certain size intervals (number distribution), or it can show how the particle area (surface distribution) or volume (volume distribution) is distributed on these intervals. Most importantly, it is fundamental to understand what distribution is measured by the available instrumentation.

The optical probe performs a line sampling of the flow field. It hence measures characteristics which depend on the projected area of the drops. Assuming spherical drops and spatial homogeneity of the drop population in the region surrounding the probe, a drop surface (interfacial area) distribution is hence collected ([14], [15]). The number and volume (or mass) drop distributions can be easily obtain multiplying the surface distribution by $1/d$ or d^2, respectively.

4.2.4. Definition of relevant drop length scales

In order to characterize the drop flow field, it is convenient to define characteristic length scales that are relevant to our problem. The following drop diameters were considered:
-   The arithmetic mean of the drop number distribution.
-   The arithmetic mean of the drop surface distribution (Sauter mean), relevant to drop/vapor heat and mass transfer (e.g. under post-dryout conditions).
-   The arithmetic mean of the drop volume/mass distribution (de Brouckere mean), relevant to drop/film mass exchange under annular flow conditions.
-   The minimum drop diameter, above which 99% of the total drop mass is contained (hence below this value the drop mass is insignificant)

- The maximum drop diameter, below which 99% of the total drop mass is contained (hence above this value the drop mass is insignificant)

An example of measured chord length distribution and resulting drop diameter distribution (Equation (8)) are plotted in Figure 6. For this particular case, the minimum diameter is about 0.2 mm, the arithmetic mean diameter is about 0.3 mm, the Sauter mean diameter is about 0.7 mm, the de Brouckere mean diameter is about 1.2 mm and the maximum diameter is about 5.3 mm.
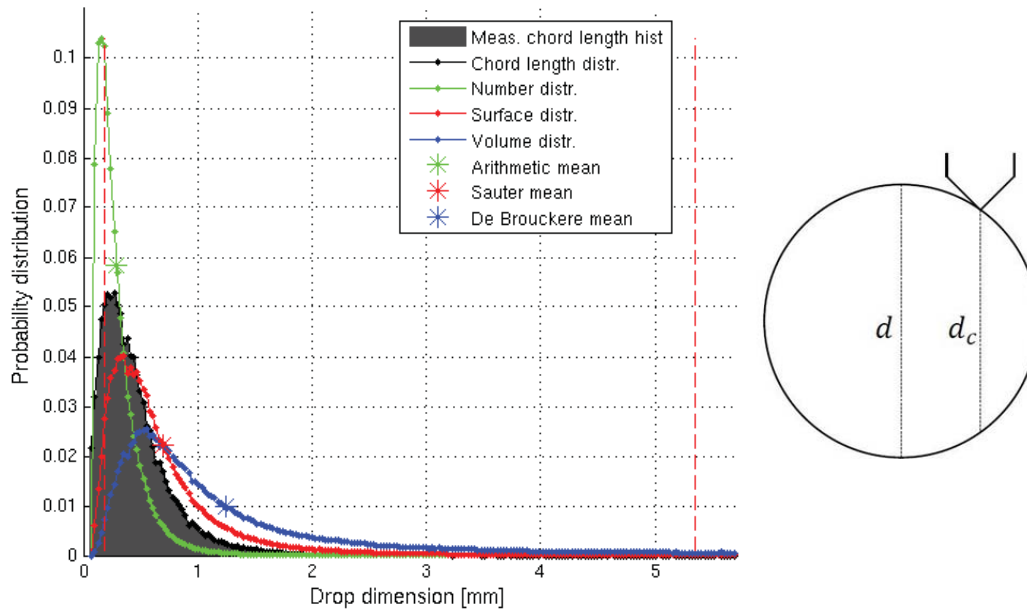

Figure 6. Example of drop chord length (measured/fitted) and diameter (number/surface/volume) distributions. Min and max diameters are shown with vertical dashed red lines

It can be observed that the surface and volume distributions are smoothly decreasing toward 0 on the low diameter side and are hence well captured by the instrumentation. The number distribution, on the other hand, might not be well captured (sharp decrease) caused by limitations due to the probe finite size and acquisition speed. Even though a significant number of small drops may be missing from the measured distributions, these drops do not have a significant contribution to the interfacial area and volume (and hence mass) of the drop field. This is confirmed by observing that the minimum drop diameter (as defined above) is higher than the mode (most probable diameter) of the drop number distribution.

4.2.5. Measurement uncertainties

The averaged Pitot dynamic pressure measurements are calculated with a standard deviations about 7% in the low dynamic pressure range (2 kPa) down to 1% in the high dynamic pressure range (40 kPa). This results in a velocity measurement uncertainty about 0.2 m/s across the whole range.

The optical probe measurements are based on an average of a large amount of drop residence times, typically collected over 20 sec. Due to the high interference frequency (between about 100 to 7000 Hz, see Section 5), the measurement sample is hence between 2000 to 130000 drops. When plotting the cumulative average of the measured void fraction (Figure 7), the precision accuracy can be estimated to be less than 0.1% void after 2000 drops.
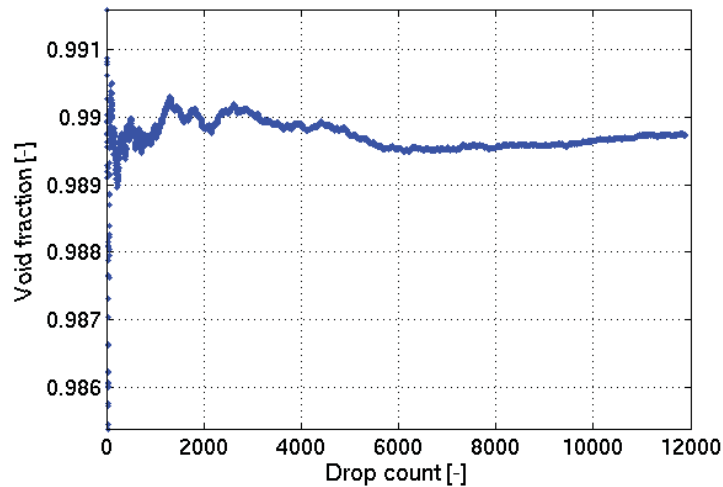
Figure 7. Cumulative average void fraction vs drop count

The algorithm to calculate the drop diameter distribution was verified using a simulated phase indicator signal from a very large sample of drops with imposed drop diameter distribution and velocity (using a Monte-Carlo technique documented in [17], applied to a single-sensor probe). In general, the arithmetic mean drop diameter was predicted with an error less than 5%. For a smaller sample, however, the error could be larger, up to 10% for a sample size of 1400 drops [16].

5. RESULTS

Pitot and optical probe measurements are presented in this section for selected FRIGG tests. The test geometry consists of a 5x5 rod bundle, including part-length rods. The measurements are performed at EOHL where the bundle hydraulic diameter is about 11 mm. The spacer grids have no mixing vanes. The measured void fraction, velocity, volumetric interfacial area and drop interference frequency are plotted as function of quality and (cross-section averaged) superficial steam velocity in Figure 8 and Figure 9, respectively. The drop diameters (minimum, arithmetic mean, Sauter mean, de Brouckere mean and maximum) are plotted as function of quality and (cross-section averaged) superficial steam velocity in Figure 10. The superficial steam velocity is the hypothetical velocity calculated as if the steam were the only phase flowing in the test section. In the case of high void fraction, it is hence nearly equal to the actual cross-section averaged steam velocity.

All measurements are presented at steady-state dryout power (for the considered test bundle) and EOHL, in the region above part-length rods. Additional data under nominal and transient operating conditions were also collected (not presented in this paper).
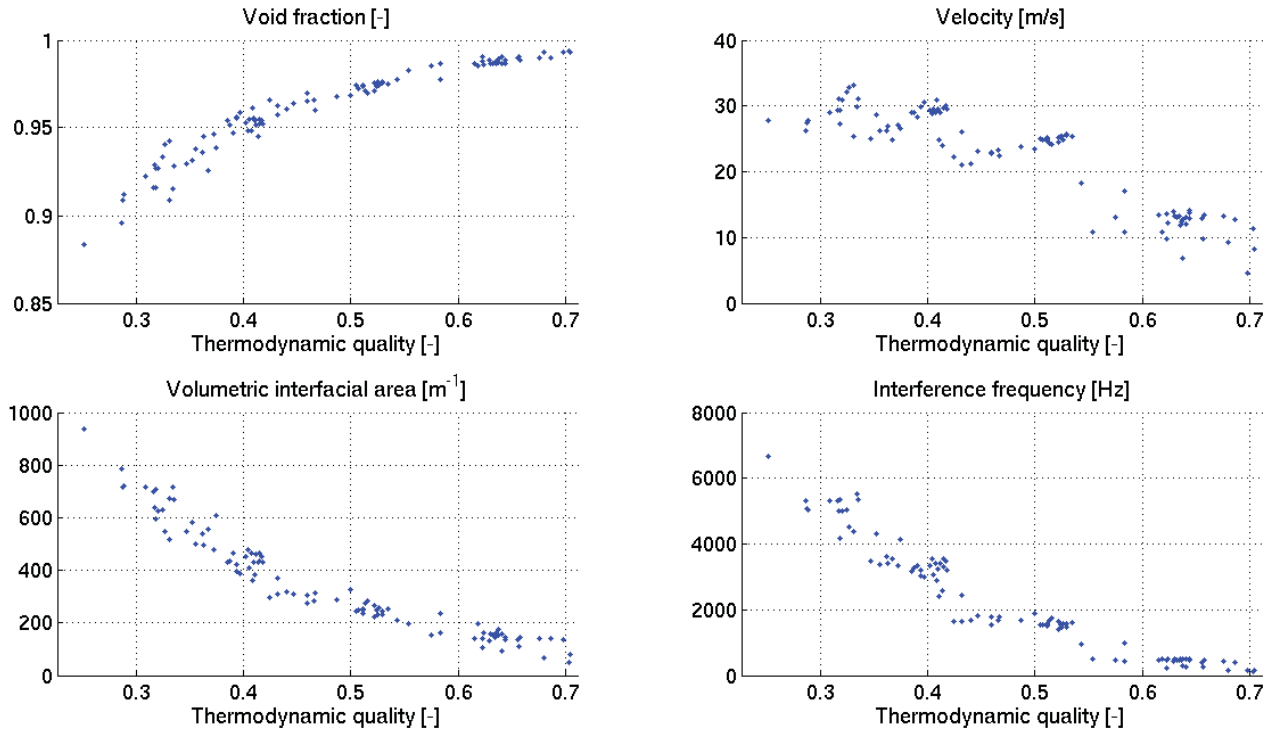
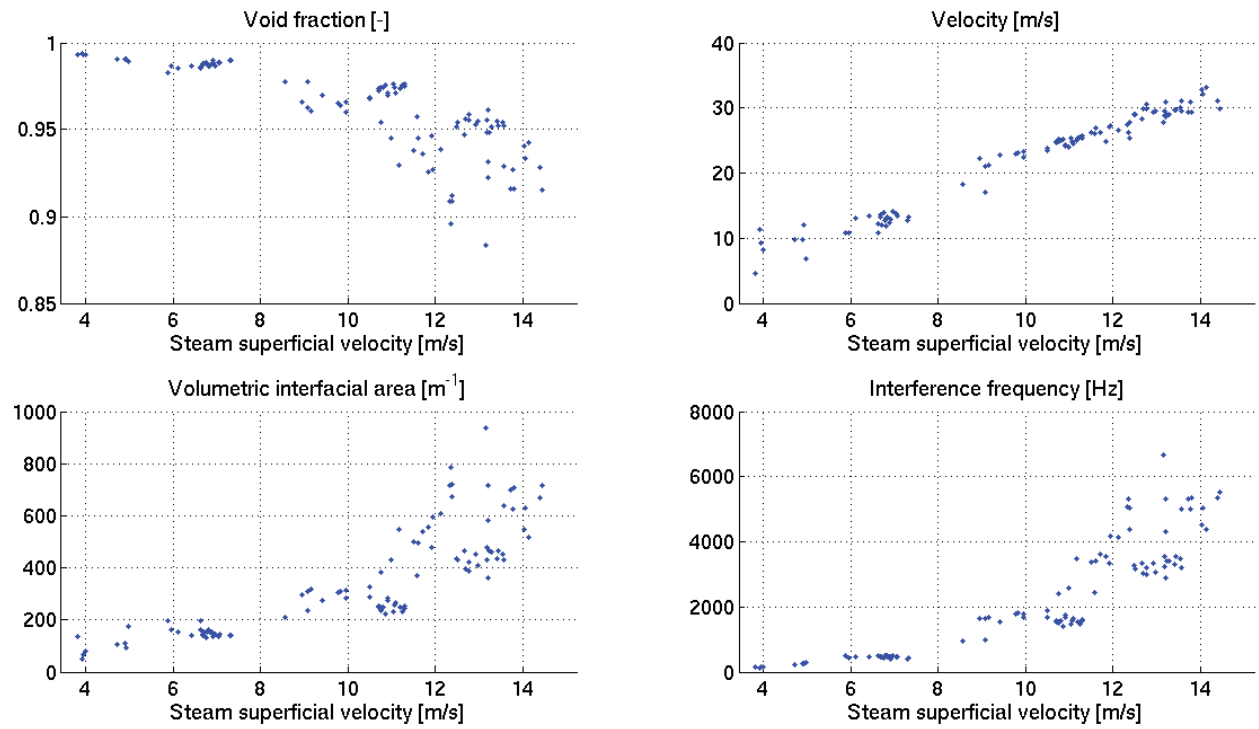**Figure 8. Local two-phase flow parameters vs. quality**

Figure 9. Local two-phase flow parameters vs. superficial steam velocity
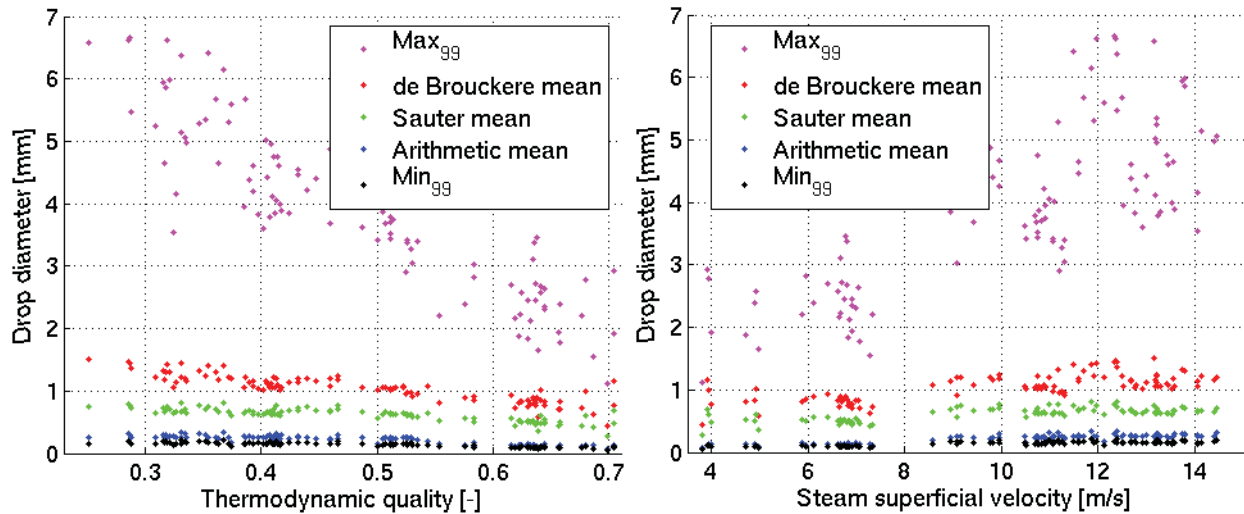
Figure 10. Drop diameters vs. quality (left) and superficial steam velocity (right)

The results show that the measured void fraction yields a typical curved shape when plotted against the (cross-section averaged) quality and that the measured velocity linearly increases with the superficial steam velocity. Other observations are as follows:

- The measured void fraction in the steam core is relatively high (0.90 – 0.99) for the corresponding quality. Considering that this region of the bundle is open (above part-length rods), it means that the steam content has drifted toward this open region. This is consistent with well-known observations in non-homogeneous geometries, which indicates that the vapor seeks the less obstructed, high velocity region of fuel lattices [18].
- The measured flow velocity is also relatively high (up to 35 m/s) and about twice the value of the superficial velocity, compensating for the low wall friction in the open region and low mixture density (high void).
- The measured drop diameters have only small dependencies with the velocity and quality, within the considered range, Figure 10. This does not agree with observations from low pressure measurements [16] where the drop diameter was noted to depend on velocity to an estimated power of -1.1. However, the maximum drop diameter seems to vary rapidly across the measured ranges.
- The measured arithmetic and Sauter mean drop diameters are about 0.3 and 0.7 mm, respectively. This is larger than expected when comparing with available low pressure measurements summarized in [16]. However, the measured Sauter mean drop diameter is within the range of some data more recently compiled in [19]. Relevant comparison with previous work is limited since no other measurement of drop size under realistic BWR core conditions is available in the literature (to the authors' knowledge).
- The Sauter mean drop diameter under BWR conditions was estimated (in [20]) to be in the range 0.1-0.3 mm using the correlation developed by Kataoka *et al.* [21] and Kocamustafaogullari *et al.* [22] and in the range 0-6-0.7 mm using the correlation developed by Ambrosini *et al.* [23]. Hence, the correlation by Ambrosini *et al.* seems to provide reasonable Sauter mean diameter values and further comparisons should be performed.
- In annular two-phase flow conditions where drop entrainment/deposition is an important mass transfer mechanism (between liquid film and drop fields), the most relevant drop size is the arithmetic mean of the volume/mass distribution (i.e. de Brouckere mean diameter), not the Sauter mean diameter. Further work is needed to develop a suitable drop size correlation under BWR operating condition corresponding to this parameter.

- The assumption of spherical drop shape and negligible drop/steam slip might not be valid for the larger measured drops sizes (several mm). Further investigations could be performed e.g. by using a transition matrix A (Equation 6) developed for non-spherical drops. However, assumption regarding the drop shape (e.g. ellipsoid) would still be necessary.

6. CONCLUSIONS

The Westinghouse FRIGG thermal-hydraulics test loop facility is being continuously upgraded to meet the challenges associated with features of modern BWR fuel designs, including mixing vanes and part-length rods. New instrumentation techniques, namely Pitot tubes and optical sensors, have been successfully tested and allowed the first-time measurements of local void fraction, local velocity, drop size distribution and drop interference frequency in annular two-phase flow under BWR steady-state nominal and dryout conditions. Further development could include the measurement of drop concentration and drop mass flux. The measurements will be used to benchmark sub-channel and two-phase CFD codes for application to modern BWR fuel designs. Further analysis of the data will also allow applying a similar post-processing scheme to realistic fast transient data.

ACKNOWLEDGMENTS

REFERENCES

1. S. Andersson, L. D. Smith III, A. Hallehn and D.-Y- Sheng, "Westinghouse fuel heat transfer test facilities," *2011 Water Reactor Fuel Performance Meeting*, Chengdu, China (2011).
2. G. Windecker and H. Anglart, "Phase distribution in a BWR fuel assembly and evaluation of a multidimensional multifield model," *Nuclear Technology*, **134** (2001).
3. M. Ahnesjö, P. Andersson, J.-M. Le Corre and S. Andersson, "Tomographic reconstructions and predictions of radial void distribution in BWR fuel bundle with part-length rods," *16th International Topical Meeting on Thermal-Hydraulics* (NURETH-16), Chicago, Aug. 30th – Sept. 4th (2015).
4. O. Nylund *et al.*, "Hydrodynamic and heat transfer measurements on a full-scale simulated 36-rod BHWR fuel element with non-uniform axial and radial heat flux distribution, ASEA-ATOM (1970).
5. K.Hau and S. Banerjee, "Measurement of mass flux in two-phase flow using combinations of Pitot tubes and gamma densitometers," *AIChE Journal*, **27**, Issue 2, pp. 177–184, (1981).
6. F. A. Hamad and S. He, "Evaluation of hot-film, dual optical and Pitot tube probes for liquid–liquid two-phase flow measurements," *Flow Measurement and Instrumentation*, **21**, Issue 3, pp. 302–311 (2010).
7. A. M. C. Chan and D. Bzovey, "Measurement of mass flux in high temperature high pressure steam-water two-phase flow using a combination of Pitot tubes and a gamma densitometer," *Nucl. Eng. Des.*, **122**, pp. 95-104 (1990).
8. A. J. White and J. B. Young, "Loss Measurements and Interpretation of Pitot Pressures in Two-Phase Vapor-Droplet Flow," *Exp. Therm. Fluid Sci.*, **15**, pp. 279-287, 1997.
9. J. M. Delhaye, J. P. Galaup, "Measurement of local void fraction in Fréon 12 with a 0.1 mm optical fiber probe," European Two-Phase Flow Meeting, Harwell (1974).
10. J. Garnier, E. Manon and G. Cubizolles, "Local measurements on flow boiling of refrigerant 12 in a vertical tube," *Multiphase Science and Technology*, **13**, no. 1-2, pp. 1–111 (2001).
11. J.-M. Le Corre, E. Hervieu, M. Ishii and J.-M. Delhaye, "Benchmark and improvements of measurement techniques for local time-averaged two-phase flow parameters," *Experiments in Fluids*, **35**, pp. 448-458 (2003).

12. J. M. Delhaye, R. Charlot, F. Danel and J. Arnault, "An optical probe for interface detection at high pressure (180 bar) and high temperature (360 C)," *Thermal-Hydraulics of Nuclear Reactors*, **2**, Merilo, M., Ed., ANS, pp. 1427-1430 (1983).

13. M. Li and D. Wilkinson, "Determination of non-spherical particle size distribution from chord length measurements. Part 1: Theoretical analysis," *Chem. Eng. Sci.*, **60**, 3251–3265 (2005).

14. G. Cubizolles, *Etude stéréologique de la topologie des écoulements diphasiques à haute pression*, Doctoral dissertation, Ecole central de Lyon, 1996.

15. J. C. Russ, R. T. Dehoff, *Practical Stereology*, 2nd edition, Plenum Press, New York, 2001.

16. B. J. Azzopardy, "Drops in annular two-phase flow," *Int. J. Multiphase Flow*, **23**, Suppl., pp. 1-53 (1997).

17. J.-M. Le Corre and M. Ishii, "Numerical evaluation and correction method for multi-sensor probe measurement techniques in two-phase bubbly flow," *Nucl. Eng. Des.*, **216**, pp 221-238 (2002).

18. R. T. Lahey, Jr. and F. J. Moody, *The Thermal-Hydraulics of a Boiling Water Reactor*, pp. 170, 2nd Edition, American Nuclear Society, La Grange Park, Illinois, USA (1980).

19. D. Caraghiaur and H. Anglart, "Drop deposition in annular two-phase flow calculated with Lagrangian particle tracking," *Nucl. Eng. Des.*, **265**, pp. 856-866 (2013).

20. H. Xie, S. Koshizuka and Y. Oka, "Numerical simulation of liquid drop deposition in annular-mist follow regime of Boiling Water Reactor," *Journal of Nuclear Science and Technology*, 41:5, 569-578 (2004).

21. I. Kataoka, M. Ishii, K. Mishima, "Generation and size distribution of droplet in annular two-phase flow," *Trans. ASME J. Fluids Eng.*, **105**, 230 (1983).

22. G. Kocamustafaogullari, S. R. Smits, J. Razi, "Maximum and mean droplet sizes in annular two-phase flow," *Int. J. Heat Mass Transfer*, **37**, 955 (1994).

23. W. Ambrosini, P. Andreussi, B. J. Azzopardi, "A physically based correlation for drop size in annular flow," *Int. J. Multiphase Flow*, **17**, 497 (1991).